International Journal of Technology 16(2) 525-535 (2025)

International Journal of Technology

http://ijtech.eng.ui.ac.id

Research Article

Using Trivalent Eu/Tb Codoped Orthophosphate Compound Mixing SiO_2 Particles to Obtain Better Color Uniformity and Luminosity for White LED

Phan Xuan Le [1], **Nguyen Thi Phuong Loan** [2*]

[1]*Faculty of Electrical Engineering Technology, Industrial University of Ho Chi Minh City, Ho Chi Minh City, 70000, Vietnam*

[2]*Faculty of Fundamental 2, Posts and Telecommunications Institute of Technology, Ho Chi Minh City, 70000, Vietnam*

[*]*Corresponding author: ntploan@ptithcm.edu.vn; Tel.: +84-937994664*

Abstract: A light-conversion phosphor composition consisting of $K_3Lu(PO_4)_2$: Tb^{3+}, Eu^{3+} (KLP:TE) phosphor, and SiO_2 particles was developed and utilized for white light-emitting diodes (WLEDs). KLP:TE phosphor was developed using a high-heat solid-state reaction. KLP:TE phosphor offers modifiable luminescence as well as an effective powershift. Fluorescent-related computations were used to evaluate KLP:TE luminescence performance. Tb^{3+}/Eu^{3+} doping ratio plays an important role in controlling the powershift between ions of Tb^{3+} and Eu^{3+}, primarily through electric dipole-dipole (d-d) achieving a high PS effectiveness of approximately 98.36%. Subsequently, KLP:TE@SiO_2 was integrated into an ultraviolet (UV) LED (light-emitting diode) package. While phosphor concentration remained constant, SiO_2 concentration varied. As a result, the performance of WLEDs was effectively regulated with SiO_2 concentration modification. The device generates white illumination with higher luminosity and color-distribution uniformity with higher SiO_2 doping concentration. It is possible to use this emerging phosphor for high-power WLEDs implementations.

Keywords: Band space; Color-distribution uniformity; Phosphor; Power transition; Warm WLED

1. Introduction

Phosphor-converted white light-emitting diodes (WLEDs) exhibit several outstanding characteristics, including high power converting effectiveness, hue adjustability, long lifespan, small size, environmental friendliness, and dependability (Anh and Lee, 2024; Le et al., 2024). These qualities enable WLEDs as a viable replacement for traditional incandescent and fluorescent lamps, and a typical WLEDs consists of two main components. The first is a blue or near-ultraviolet (NUV) LED (light-emitting diode) chip, while the second includes at least one phosphor material derived from rare-earth-doped compounds (Tung et al., 2024; My et al., 2022; Le et al., 2022). Phosphor plays an important role in determining the total illuminating effectiveness, hue reproduction, and heat steadiness of the resulting white illumination, making it a crucial element (Tran et al., 2020a; 2020b; Loan et al., 2020). Until recently, the most common and straightforward approach to fabricating commercial WLEDs involved the addition of a yellow phosphor $Y_3Al_5O_{12}$:Ce^{3+} (YAG: Ce) to one blue LED chip (Jia et al., 2016). However, white illumination generated from the device developed has a color deficiency in the green as well as red areas, which severely restricts its wide-scale applicability and results in deficient chromatic rendering indices (CRI<80) and cold-white light due to highly correlated chromatic temperature (CCT>4500 K) (Dang et al., 2021).

https://doi.org/10.14716/ijtech.v16i2.6173
Received November 2022; Revised May 2023; Accepted July 2023

In order to improve the effectiveness of WLEDs, there is a need to enhance the green or red radiation proportion (Thai et al., 2023). According to an investigation, red phosphors are known to execute better red emission for the white light spectrum (Hu et al., 2023). Another report showed red-light improvement, the luminescence was occasionally degraded, and CRI did not reach the expected value (Huu et al., 2022). One of the problems with such results is that the available red phosphors on the market give an inadequate red emission band for high-color rendering tasks.

The traditional InGaN blue chip has several challenges, including the reduction in efficiency and excessively emitted blue light (Verzellesi et al., 2013). These problems can be mitigated by replacing the blue-emitting InGaN chip with an ultraviolet (UV)-violet chip (Loan et al., 2021). In the last decades, the industry has been transitioning toward the adoption of high-power UV LED. This LED type has been applied in many sectors, such as medical diagnostics, imaging, spectroscopy, biosensing, and material curing (Kneissl et al., 2019; Widiyati and Poernomo, 2018). However, phosphor performances are often unstable and degraded under high-power operation (Kim et al., 2017). Therefore, research topics focus on generating red phosphors for the development of LED devices with a great CRI as well as acceptable CCT. In these conditions, it is important to investigate tri-hue light-emitting phosphors that are effectively stimulated through NUV radiation while meeting the requirements for WLEDs devices (Kazakovsky et al., 2020; Desnijder et al., 2019).

Due to their exceptional luminous qualities and distinct emitting ranges, rare-earth (RE) ions play an important in current display illumination, photodetection, optic amplification, and other relevant applications. It is well known that the central RE ions' illumination radiation is primarily caused by the efficient power shift (PS) between the triplet condition for the ligand and the crystal field conditions (Salerno, 2021). Consequently, PS plays a crucial role in both theoretical research and practical applications related to the color tuning of phosphors. Tb^{3+} ions are the most prevalent activators in phosphors. According to the number of dopants, their radiation is the consequence of either the $^5D_3 \rightarrow {}^7F_J$ transformation inside a blue zone or the $^5D_4 \rightarrow {}^7F_J$ activity (J = 6-2) inside one green area (Thi et al., 2023). The interaction between Tb^{3+} ions becomes stronger with increasing Tb^{3+} dosage, resulting in a cross-relaxation among the $^5D_3$ as well as $^5D_4$ states along with the induction for the $^5D_4 \rightarrow {}^7F_J$ transition with mostly green radiation (Royer et al., 2019; Tian et al., 2019). However, the red element from different phosphor samples incorporated with Tb^{3+} as well as Eu^{3+} can be compensated for by the magnetic dipole transition ($^5D_0 \rightarrow {}^7F_1$) along with electric dipole transformation ($^5D_0 \rightarrow {}^7F_2$) of Eu^{3+} ions (Thi et al., 2023).

This research applied $K_3Lu(PO_4)_2$:Tb^{3+},Eu^{3+} phosphor (KLP:TE) to create a UV-LED package. $K_3Lu(PO_4)_2$ was selected as the host material, while $(PO_4)_3$- orthophosphates are known to be a good phosphor group for doping Eu^{3+} and Tb^{3+}. These incorporations can offer extremely efficient high-power transformation and UV-energy absorption (Wu et al., 2020; Choi et al., 2019). A novel high-heat solid-state KLP:TE phosphor yielding controllable emission in the orange-red region was developed. Then, the phosphor was mixed with the original phosphor composition containing YAG:Ce^{3+} and silicone gel in order to improve the red-light spectrum. SiO_2 particles were added to obtain significant scattering improvement in the WLEDs package. The luminescence computation of the created KLP:TE phosphor was described. Subsequently, LED light performance was demonstrated in the presence of KLP:TE@SiO_2 composition. The concentration of KLP:TE was fixed while varying SiO_2 doping amounts. This regulation of the scattering effect increases the likelihood of achieving enhanced color uniformity, rendering efficiency, and luminous output in WLEDs. The reported data demonstrate promoted luminous flux and notable color-deviation decrease when increasing the SiO_2 doping amount. However, the chromatic rendering results do not meet the expectations due to the lack of green and deeper red regions to achieve the full-chromatic spectrum for the generation of white light. The results demonstrated the application possibility for KLP:TE@SiO_2 in UV WLEDs in terms of accomplishing improved color-distribution uniformity and luminosity.

2. Experimental Section

2.1. Substances and combination

The typical high-temperature solid-state reaction was used to create KLP:TE phosphor. Concentrations of Tb^{3+} and Eu^{3+} ions were determined at 0.1 and 0.06 mol, respectively. The materials required for the development process with steps carried out during the process are shown in Table 1 (Sheu et al., 2019).

Table 1 Constituents and creation process of $K_3Lu(PO_4)_2$: Tb^{3+}, Eu^{3+}

Materials	Purity	Process
K_2CO_3	99%	- All materials are weighed with predetermined amounts.
Lu_2O_3	99.99%	- These powders are homogeneously mixed and ground in one agate mortar.
$NH_4H_2PO_4$	99%	- The attained composition is pre-heated at 800◦C in 4 hours.
Tb_4O_7	99.99%	- The composition is then sintered at 1150◦C for 4 hours in a muffle furnace in the air surrounding.
Eu_2O_3	99.99%	- After that, the obtained sample was removed and allowed to cool at normal temperature.
K_2CO_3	99.99%	- The sample was pulverized to acquire powders ready for WLEDs creation.

2.2. LED manufacture

KLP:TE concentration was fixed and blended with $YAG:Ce^{3+}$ phosphor, and SiO_2 particles in silicone. The powder combination was combined with one UV chip (1 W, ex = 365 nm) and OE6550 silica gel in the form of a fixing agent to develop WLEDs (Tanaka et al., 2021). Figure 1 below shows the WLEDs simulation carried out during the tests. The concentration of SiO_2 is modified in the range of 0-25 wt.%.

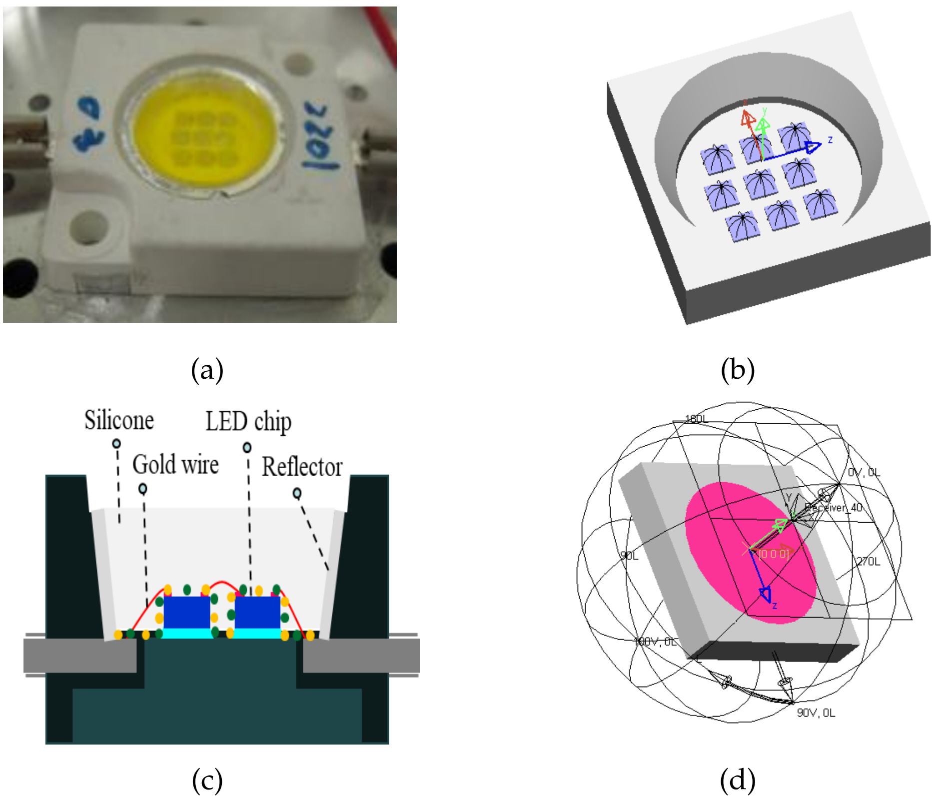

Figure 1 WLEDs formation depictions: (a) WLEDs device, (b) Binding schema, (c) Illustrated device, (d) Recreated device in program LightTools

2.3. Characterization

Following the development process of KLP:TE samples, their characteristics were examined. For this task, various tools were used, and the characteristics as well as their matching tools are shown in Table 2 (Li et al., 2021, Li and Zhen, 2020).

Table 2 Characteristics and Determining Tools

Characteristics	Tools
XRD patterns	D8 Advance diffractometer with Cu-Kα tube and a voltage reaching 40 kilovolts as well as current reaching 30 milliamperes
Rietveld refinement	GSAS program
Chemical blends along with element valence	XPS using an ESCALAB Xi+ electron spectrometer
Diffuse reflectance spectra	UV-Vis-NIR spectrophotometer
Photoluminescent excitation/emission spectra	Fluorescence spectrophotometer accompanied by Xe light (400 V, 150 W)
Quantum performance	Spectrofluorometer with a 150 W xenon light source
Fluorescent degradation arches	FS5 spectrofluorometer accompanied by 150-W CW Xe arc light with no ozone

3. Results and Discussion

3.1. Luminescent computation of phosphor

With the exception of Ce^{3+}, most trivalent rare earth ions produce a series of relatively narrow emission lines due to intrinsic $4f^n$ -$4f^n$ shifts barely influenced by the base's molecule. However, the host plays a part in the discharge characteristics in the 4f-4f dischargers because it affects the relative potency of the discharge lines (through local symmetry-related picking principles). The splitting of the emission lines in dependence on the crystal field, and the quantum efficiency (by virtue of the existence of non-radiative pathways and temperature abatement). Certain rare earth ions generate rays that may be seen. Notable rare earth ions include Tb^{3+} (green discharge, main apex under 545 nm) as well as Eu^{3+} (orange to red discharge, key maximum around 600 or 620 nm), which have both been extensively used in cathode ray tubes and fluorescent light phosphors. Since 5d states, along with charge transfer conditions (CTC), typically lie below 350 nm, the primary challenge in adapting these materials for LED applications is the lack of efficient and broad emission pathways in the near-UV to blue spectral region.

By sensitizing with the proper addition of co-dopants, the recreation spectrum may extend toward greater wavelengths. For instance, the addition of Ce^{3+} may sensitize Tb^{3+} discharge. There were reports of extra (wide band) routes for Eu^{3+} being created by the addition of Bi^{3+}. As previously mentioned, narrow-line emission under 460, 540, as well as 610 nm may be combined to provide effective white light emission, WLEDs can be designed with low color rendering quality but high illuminating efficiency. The principal emission peaks of Tb3+ and Eu3+ align with the required red and green components. Using red phosphors doped with Eu3+ helps prevent green phosphor dominance, enhancing color balance radioactivity from being absorbed again, a drawback for red phosphors made using Eu^{2+} dopant.

The host's absorbing band is primarily responsible for KLP:TE phosphors' close 200 nm absorption characteristics. The power gap can be estimated by utilizing the Kubelka-Munk function to further distinguish if $K_3Lu(PO_4)_2$ would be a direct or indirect band gap substance, demonstrated using Equation 1 (Mednikov et al., 2020):

$$[F(R_\infty)h\upsilon]^n = C(h\upsilon - E_g) \tag{1}$$

where hv is the photo energy, R_∞ represents reflectivity, and E_g stands for optic band space energy. The combination is regarded as a direct band space substance when $n = 2$. The indirect band space is indicated by $n = 12$.

Weak blue illumination emissions are produced at 417 and 438 nm by a few stimulated states of Tb^{3+} that move straight from $^5D_3$ to $^7F_6$. Other stimulated states undertake the non-radiative shift, relax towards the bottom excitation state $^5D_4$, but afterward suffer the radioactive degradation towards $^7F_6$, which emits a powerful green illumination. PS procedure among Tb^{3+}/Eu^{3+} 4f stimulated states is facilitated by the energy mismatch. The addition of Eu^{3+} to KLP:TE results in partial power transmission from $^5D_4 \rightarrow {^7F_J}$ shift between Tb^{3+} and Eu^{3+} accompanied by later alleviation towards $^5D_0$. The last orange-red emission results from the power radiation's decline from $^5D_0$ to $^7F_0$.

It is discovered that a double-exponential degradation function may suit the degradation curve nicely (Sezer et al., 2019), as shown in Equation 2:

$$It = A_1 \exp(-t/\tau_1) + A_2 \exp(-t/\tau_2) \tag{2}$$

$I(t)$ denotes Tb^{3+} emitting strengths under the delay time t; τ_1 and τ_2 denote the exponential element's fast and slow fluorescent durations; and A_1 and A_2 denote the specific constants Calculations for the median duration (τ^*) in Equation 3 (Rabaza et al., 2020):

$$\tau^* = (A_1\tau_1^2 + A_2\tau_2^2)/(A_1\tau_1 + A_2\tau_2) \tag{3}$$

In the Tb/Eu PS procedure, the transferring probability (P_{Tb-Eu}) may be represented as shown by Equation 4:

$$P_{Tb-Eu} = (1/\tau_x) - (1/\tau_0) \tag{4}$$

where τ_x and τ_0 represent the lives of Tb^{3+} with and without Eu^{3+} for the equal sensitizer doses, in turn. Subsequently, the formula below calculates the power-shift effectiveness (η_T) from ions of Tb^{3+} to Eu^{3+} can be computed with Equation 5:

$$\eta_T = 1 - (\tau_x/\tau_0) \tag{5}$$

where τ_x signifies the duration for Tb^{3+} in the co-doped Tb/Eu phosphor samples; τ_0 signifies the radiative degradation lifetime of Tb^{3+}; and T signifies the power-shift effectiveness. The transmission effectiveness increases from 26.93% to almost 100% with a rise in Eu concentration (Liao et al., 2019), as calculated using Equation 6:

$$R_c \approx 2[3V/4\pi x_c N]^{1/3} \tag{6}$$

x_c signifies the combined concentration for Tb^{3+} as well as Eu^{3+}. N signifies the formula unit amount in the unit cell. V signifies the unit cell's volume. N reaches 3, while V reaches 612.973128 Å^3 under $\eta_T = 98.36\%$, $x_c = 0.36$ (sum percentage for sensitizer Tb^{3+} as well as trigger Eu^{3+}) for $K_3Lu(PO_4)_2$ host. Therefore, the PS process should be assigned to the multipolar interaction since the associated R_c is equivalent to 10.274 Å, which is substantially bigger than 5 Å.

The multipole interaction governs the resonance PS between Tb^{3+} and Eu^{3+} from KLP:TE phosphors. Reisfeld's theory, along with Dexter's expression, presented in Equation 7, helps us assess the PS process (García et al., 2020):

$$\eta_0/\eta \approx I_{so}/I_s \propto C^{n/3} \tag{7}$$

where I_s and I_{so} signify the luminescent strengths of the sensitizer Tb^{3+} in the case of having and lacking Eu^{3+}. C signifies the Eu^{3+} presence used for incorporation. n values of 6, 8, 10 correspond to dipole-dipole (d-d), dipole-quadrupole (d-q), quadrupole-quadrupole (q-q) interactivities. η_0 and η signify the illumination quantum performance (QP).

The emitting strengths for Tb^{3+} and Eu^{3+} are reduced by thermal quenching to 68.1% and 84.0% under room temperature. Arrhenius equation, included in Equation 8, is used to calculate the trigger power (ΔE) and further evaluate the heat steadiness (Bullough et al., 2019):

$$\ln(I_o / I_T) = \ln A - \Delta E / kT \tag{8}$$

where A signifies one constant. k signifies the Boltzmann constant (8.617×10^{-5} eV K^{-1}). I_0 and I_T are the luminous strengths of KLP:TE under ambient heat and a specified heat level, accordingly.

3.2. Phosphor Influence on WLEDs performances

The concentration of SiO_2 is adjusted to impact the scattering property of the whole phosphor compound containing YAG:Ce^{3+} and KLP:TE phosphors. Scattering coefficients (SCs), regarding the increased concentration of SiO_2 from 0 wt.% to 25 wt.% in the composition, were shown in Figure 2. According to observation, high SiO_2 concentrations stimulate SCs, thereby enabling greater transmission and conversion of scattered blue-chip light into longer-wavelength light. When the forward emission exhibits an increase in dispersed blue light, coupled with a decrease in blue-light reabsorption and backscattering, such a phenomenon has the potential to enhance luminosity.

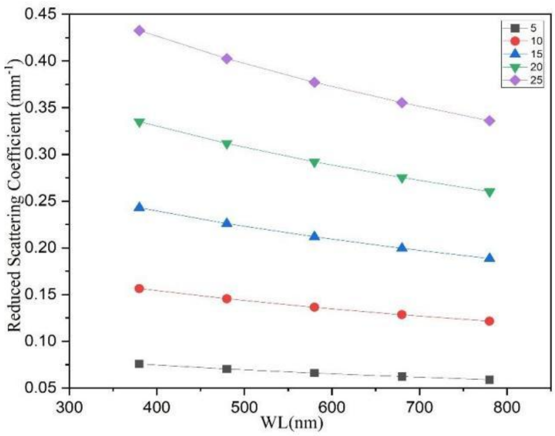

Figure 2 Scattering coefficients when varying SiO_2 contents in KLP:TE@SiO_2 composition

To achieve this objective, it is essential to maintain a lower concentration of YAG:Ce^{3+} yellow phosphor as SiO_2 concentration rises. The adjustment also contributes to minimizing fluctuations in the angular CCT range. Figure 3 shows the reduction in YAG:Ce^{3+} concentration with increasing SiO_2 concentration, and Figures 4 and 5 show the stability of CCT at higher concentrations. Furthermore, Figure 4 demonstrates how, at higher doping concentrations, the phosphor may reduce its CCT fluctuation (D-CCT). With 25wt.% SiO_2, D-CCT eventually reaches its lowest point at about 225 K, which is lower by 45 K than the value when no SiO_2 was used.

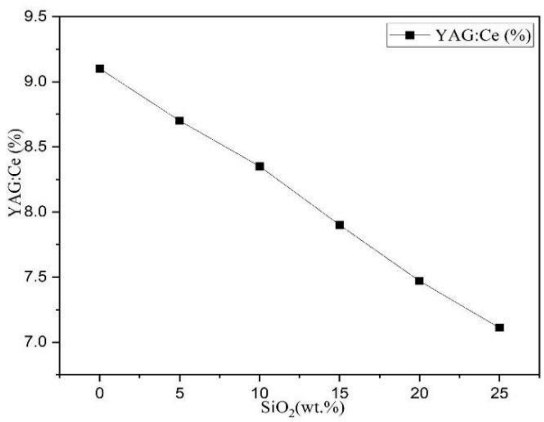

Figure 3 YGA:Ce phosphor dosage values when varying SiO_2 contents in KLP:TE@SiO_2 composition

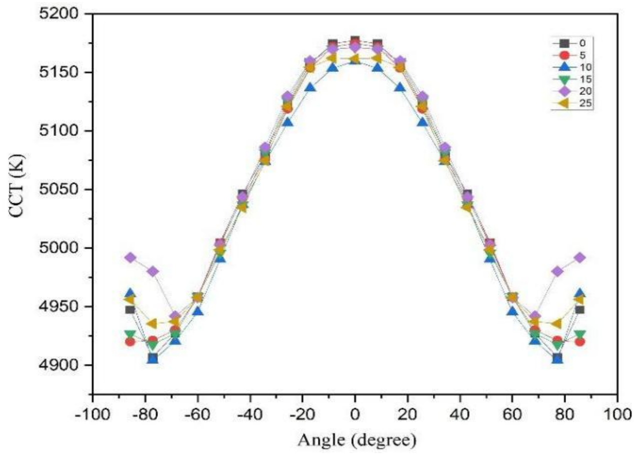

Figure 4 CCT values when varying SiO_2 contents in KLP:TE@SiO_2 composition

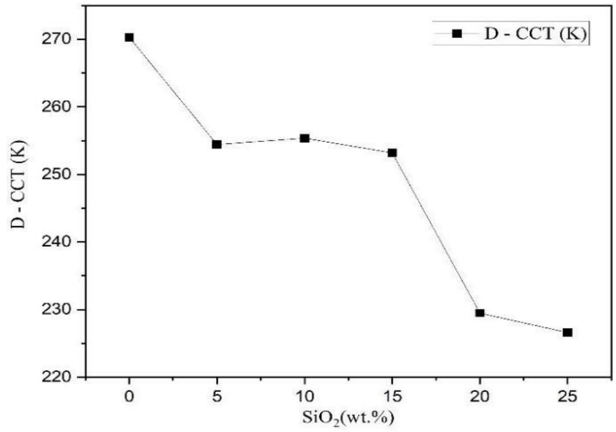

Figure 5 Color difference values when varying SiO_2 contents in KLP:TE@SiO_2 composition

Figure 6 shows how the increase in SiO_2 proportion did not always lead to an increase in the luminous brightness of white light emission. According to the results, using 0 – 5wt.% SiO_2 leads to a considerable brightness reduction while using 25wt.% SiO_2 provided the greatest luminosity. As shown in Figure 5, the D-CCT value at 25wt.% SiO_2 is the highest. This exhibits an uneven color distribution and lower blue emission intensity due to greater back-scattering and reabsorption. Higher SiO_2 doses in particular would promote the light conversion from blue to yellow or orange-red as phosphor absorbs more backscattered blue light.

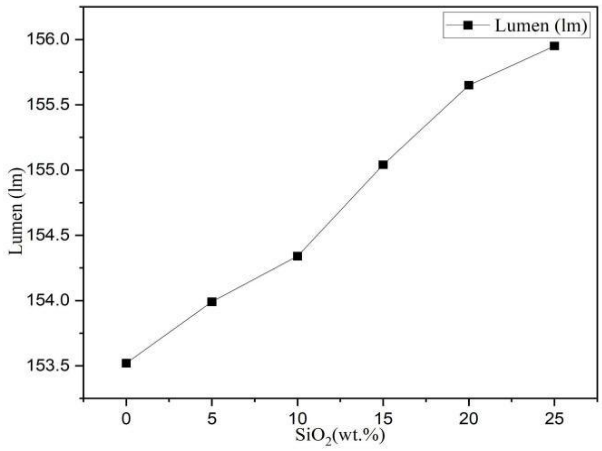

Figure 6 Luminescence strength when varying SiO_2 contents in KLP:TE@SiO_2 composition

The quantity of SiO_2 increases and leads to the thickening of the phosphor layer. This would cause the converted light to reflect off various surfaces several times, decreasing the power of the overall emission spectrum. In other words, if the dosage of SiO_2 is too high, a greater amount of converted light has the potential to be reflected, resulting in a reduction in luminous intensity and an increase in CCT values. As a result, it was determined that 25wt.% of SiO_2 was the appropriate amount for the simulated WLEDs in order to improve luminous intensity and color uniformity (Aydın et al., 2021).

The concentration of SiO_2 not only impacts the brightness but also significantly influences the color rendering performance of WLEDs. The evaluation of color rendition values through hue rendering indicators (CRI) and hue quality scale (CQS) measurements showed a consistent decline as SiO_2 concentration increased up to 25wt.% (Figures 7 and 8). The observable decreases in CRI and CQS can be attributed to imbalanced blue, green, and yellow-orange patterns. As previously mentioned, the increased scattering resulting from the higher SiO_2 dose creates an imbalance, causing the illumination emission hue to shift further toward the yellow-orange region. Consequently, excessive dispersion leads to a decrease in both CRI and CQS. Further investigations into additional characteristics of this phosphor, such as particle size, will be conducted in the ongoing research to effectively manage CRI and CQS (Oliveira et al., 2019).

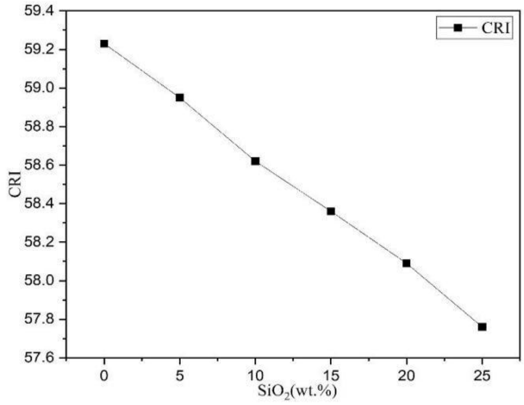

Figure 7 CRI values of WLEDs when varying SiO_2 contents in KLP:TE@SiO_2 composition

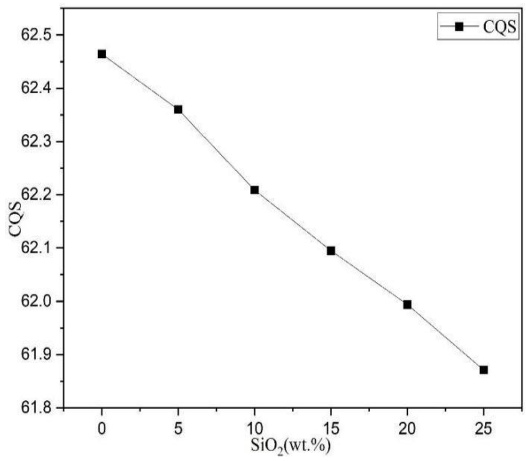

Figure 8 CQS values when varying SiO_2 contents in KLP:TE@SiO_2 composition

The emission spectra of KLP:TE@SiO_2 phosphor-based WLEDs are shown in the supplementary materials section. The entire white emission band demonstrated how phosphor may increase the power of blue and orange-red radiation. The highest emission points may be observed in the blue (450 nm) and yellow-orange (600 nm) areas. This can be attributed to the effect of scattering improvement provided by SiO_2 presence in the phosphor compound. Particularly, lighting efficiency may be changed by modifying SiO_2 amount settings to alter the scattering and absorption patterns of WLEDs light output. When higher SiO_2 is introduced, scattering productivity is more active, leading to higher light absorption of the phosphor compound. Therefore, UV-light utilization by KLP:TE phosphor is probably simulated, resulting in better conversion for blue light and orange-red light related to the trivalent Tb and Eu ions.

4. Conclusions

In conclusion, this research successfully developed and utilized a light-conversion phosphor compound containing $K_3Lu(PO_4)_2$: Tb^{3+}, Eu^{3+} orange-red phosphor, SiO_2 particles, and YAG:Ce^{3+} yellow phosphor for WLEDs using UV chip. KLP:TE phosphor was synthesized through a high-heat solid-state reaction, offering adjustable luminescence properties and effective powershift capabilities. The electric d-d interaction was found to contribute to an elevated powershift effectiveness of approximately 98.36%. Subsequently, the illumination properties of WLEDs were controlled with SiO_2 concentration modification. It is possible to induce higher luminosity and improved color-distribution uniformity by increasing SiO_2 doping concentrations. Either CRI or CQS reduces with a highly doped SiO_2 amount in the phosphor compound. In general, this emerging phosphor composition showed great potential for high-power WLEDs applications, offering the ability to generate white illumination with enhanced brightness and uniformity. Further exploration and utilization of this phosphor composition could lead to significant advancements in high-power WLEDs implementations.

Acknowledgements

The authors would like to thank Professor Hsiao-Yi Lee, National Kaohsiung University of Science and Technology, for providing software and experiment support.

Author Contributions

Phan Xuan Le: Conceptualization, Methodology, Software, Validation, Investigation, Resources, Data Curation, Writing, Review, Editing, Visualization, Supervision, Project administration

Nguyen Thi Phuong Loan: Conceptualization, Methodology, Software, Validation, Investigation, Resources, Data Curation, Writing, Review, Editing, Visualization

Conflict of Interest

The authors declare no conflicts of interest.

References

Anh, NDQ & Lee, HY 2024, 'Titanium dioxide in vanadate red phosphor compound for conventional white light emitting diodes', *Optoelectronics and Advanced Materials - Rapid Communications*, vol. 18, no. 9-10, pp. 480-484

Aydin, E, Liu, J, Ugur, E, Azmi, R, Harrison, GT, Hou, Y, Chen, B, Zhumagali, S, De Bastiani, M, Wang, M, Raja, W, Allen, TG, Rehman, AU, Subbiah, AS, Babics, M, Babayigit, A, Isikgor, FH, Wang, K, Van Kerschaver, E, Tsetseris, L, Sargent, EH, Laquai, F & De Wolf, S 2021, 'Ligand-bridged charge extraction and enhanced quantum efficiency enable efficient n–i–p perovskite/silicon tandem solar cells', *Energy & Environmental Science*, vol. 14, no. 8, pp. 4377–4390, https://doi.org/10.1039/d1ee01206a

Bullough, JD, Bierman, A & Rea, MS 2019, 'Evaluating the blue-light hazard from solid state lighting', *International Journal of Occupational Safety and Ergonomics*, vol. 25, no. 2, pp. 311–320, https://doi.org/10.1080/10803548.2017.1375172

Choi, S, Kim, C, Suh, JM & Jang, HW 2019, 'Reduced graphene oxide-based materials for electrochemical energy conversion reactions', *Carbon Energy*, vol. 1, no. 1, pp. 85–108, https://doi.org/10.1002/cey2.13

Dang, HP, That, PT & Anh, NDQ 2021, 'Utilizing $CaCO_3$, CaF_2, SiO_2, and TiO_2 phosphors as approaches to the improved color uniformity and lumen efficacy of WLEDs', *Telkomnika*, vol. 19, no. 2, pp. 623-630, https://doi.org/10.12928/TELKOMNIKA.v19i2.16357

Desnijder, K, Deketelaere, W, Ryckaert, W, Hanselaer, P & Meuret, Y 2019, 'Efficient Design Method of Segmented Lenses for Lighting Applications with Prescribed Intensity and Low Peak Luminance', *LEUKOS* *the Journal of the Illuminating Engineering Society of North America*, vol. 15, no. 4, pp. 281–292, https://doi.org/10.1080/15502724.2018.1517599

García, M, North, P, Viana-Soto, A, Stavros, NE, Rosette, J, Martín, MP, Franquesa, M, González-Cascón, R, Riaño, D, Becerra, J & Zhao, K 2020, 'Evaluating the potential of LiDAR data for fire damage assessment: A radiative transfer model approach', *Remote Sensing of Environment*, vol. 247, pp. 111893, https://doi.org/10.1016/j.rse.2020.111893

Hu, X, Zhang, A, Sun, H, Zeng, F, Lei, Y, Xie, L, Yu, R, Deng, B & Lin, H 2023, 'Novel red-emitting $Sr_3LaTa_3O_{12}$:Eu^{3+} phosphor with high color purity and stability for w-LEDs and visualization of latent fingerprint', *Journal of Luminescence*, vol. 258, article 119806, https://doi.org/10.1016/j.jlumin.2023.119806

Huu, PD & Thi, DAN 2022, 'Selection of multi-layer remote phosphor structure for heightened chromaticity and luminous performance of white light-emitting diodes', *International Journal of Technology*, vol. 13, no. 4, pp. 837-847, https://doi.org/10.14716/ijtech.v13i4.5051

Jia, J, Zhang, A, Li, D, Liu, X, Xu, B & Jia, H 2016, 'Preparation and properties of the flexible remote phosphor film for blue chip-based white LED', *Materials & Design*, vol. 102, pp. 8-13, https://doi.org/10.1016/j.matdes.2016.04.022

Kazakovsky, NT, Korolev, VA & Yukhimchuk, AA 2020, 'New technologies of liquid radioactive waste conditioning', *Fusion Science and Technology*, vol. 76, no. 3, pp. 191-193, https://doi.org/10.1080/15361055.2019.1689892

Kim, YH, Viswanath, NSM, Unithrattil, S, Kim, HJ & Im, WB 2017, 'Review—Phosphor plates for high-power LED applications: Challenges and opportunities toward perfect lighting', *ECS Journal of Solid State Science and Technology*, vol. 7, no. 1, pp. R3134-R3147, https://doi.org/10.1149/2.0181801jss

Kneissl, M, Seong, TY, Han, J & Amano, H 2019, 'The emergence and prospects of deep-ultraviolet light-emitting diode technologies', *Nature Photonics*, vol. 13, no. 4, pp. 233–244, https://doi.org/10.1038/s41566-019-0359-9

Le, PX, Anh, NDQ & Lee, HY 2024, 'Regulating the white LED properties with different SiO_2 particle sizes', *Optoelectronics and Advanced Materials - Rapid Communications*, vol. 18, no. 9-10, pp. 485-489

Le, PX, Trang, TT, Anh, NDQ, Lee, HY & Tho, LV 2022, 'Comparison between SEPs of $CaCO_3$ and TiO_2 in phosphor layer for better color uniformity and stable luminous flux of WLEDs with 7000K', *Materials Science Poland*, vol. 40, no. 1, pp. 1–8, https://doi.org/10.2478/msp-2022-0008

Li, F, Zhao, Y, Gao, H, Wang, D, Miao, Z, Cao, H, Yang, Z & He, W 2021, 'Doping white carbon black particles to adjust the electro-optical properties of PDLC', *Liquid Crystals*, vol. 48, no. 15, pp. 2130-2139, https://doi.org/10.1080/02678292.2021.1931971

Li, K & Zhen, W 2020, 'Performance, structure-property relationship and biodegradability of poly(lactic acid)/amide ammonium acetate organic vermiculite intercalation nanocomposites', *Polymer-Plastics Technology and Materials*, vol. 59, no. 7, pp. 702-721, https://doi.org/10.1080/25740881.2019.1686763

Liao, C, Chiu, H & Hsieh, Y 2019, 'Wide-range dimmable LED lighting based on QL-SEPIC converter', *EPE Journal*, vol. 29, no. 1, pp. 25-37, https://doi.org/10.1080/09398368.2018.1494671

Loan, NTP & Anh, NDQ 2020, 'The application of double-layer remote phosphor structures in increasing WLEDs color rendering index and lumen output', *International Journal of Electrical and Computer Engineering*, vol. 10, no. 5, pp. 5183-5190, https://doi.org/10.11591/ijece.v10i5.pp5183-5190

Loan, NTP & Anh, NDQ 2021, 'Enhancing optical performance of dual-layer remote phosphor structures with the application of $LAASO_4$:Eu^3+ and Y_2O_3:Ho^3+', *Optoelectronics and Advanced Materials - Rapid Communications*, vol. 15, no. 1-2, pp. 71–78

Mednikov, SV, Valo, AV & Ponomarev, AS 2020, 'Photochromic effect in piezoelectric ceramics PZT-19', *Ferroelectrics*, vol. 561, no. 1, pp. 36-43, https://doi.org/10.1080/00150193.2020.1736911

My, LTT, Thai, NL, Bui, TM, Lee, HY & Anh, NDQ 2022, 'Phosphor conversion for WLEDs: YBO_3:Ce^3+, Tb^3+ and its effects on the luminous intensity and chromatic properties of dual-layer WLED model', *Materials Science Poland*, vol. 40, no. 4, pp. 105–113, https://doi.org/10.2478/msp-2022-0050

Oliveira, MAB, Scop, M, Abreu, ACO, Sanches, PRS, Rossi, AC, Noguera, AD, Calcagnotto, ME & Hidalgo, MP 2019, 'Entraining effects of variations in light spectral composition on the rest-activity rhythm of a nocturnal rodent', *Chronobiology International*, vol. 36, no. 7, pp. 934-944, https://doi.org/10.1080/07420528.2019.1599008

Rabaza, O, Lorente, DG, Pozo, AM & Ocón, FP 2020, 'Application of a differential evolution algorithm in the design of public lighting installations maximizing energy efficiency', *LEUKOS*, vol. 16, no. 3, pp. 217-227, https://doi.org/10.1080/15502724.2019.1568255

Salerno, E 2021, *Synthetic and spectroscopic investigations of ligand field effects in molecular lanthanide ion complexes,* Doctoral dissertation, Deep Blue, University of Michigan, US, https://doi.org/10.7302/2652

Sezer, T, Altinisik, M, Guler, EM, Kocyigit, A, Ozdemir, H & Koytak, A 2019, 'Evaluation of xenon, light-emitting diode (LED) and halogen light toxicity on cultured retinal pigment epithelial cells', *Cutaneous and Ocular Toxicology*, vol. 38, no. 2, pp. 125-130, https://doi.org/10.1080/15569527.2018.1539008

Sheu, M, Liu, Y, Wang, J & Pan, J 2019, 'Design of a bi-directional illumination system for a dual view capsule endoscope', *Journal of Modern Optics*, vol. 66, no. 3, pp. 252-262, https://doi.org/10.1080/09500340.2018.1516829

Tanaka, M, Yamada, T, Shigeta, M, Komen, H, Fukahori, M & Saito, N 2021, 'Experimental study on effects of gas-shielding in lap-fillet arc welding', *Welding International*, vol. 35, no. 10-12, pp. 492-507, https://doi.org/10.1080/09507116.2021.1980296

Thai, NL, Bui, TM, Le, AT & Thi, DAN 2023, 'Utilization of BaAl1.4Si0.6O3.4N0.6:Eu2+ green-emitting phosphor to improve luminous intensity and color adequacy of white light-emitting diodes', *International Journal of Technology*, vol. 14, no. 1, pp. 119-128, https://doi.org/10.14716/ijtech.v14i1.5666

Thi, MHN, Thai, NL, Bui, TM & Ho, SD 2023, 'The light features and Bredigite layout for orthosilicate phosphor in WLED devices', *International Journal of Technology*, vol. 14, no. 4, pp. 911-920, https://doi.org/10.14716/ijtech.v14i4.5785

Thi, MHN, Thai, NL, Bui, TM & Thao, NTP 2023, 'Ca8MgY(PO4)7:Eu2+,Mn2+: A promising phosphor in near-ultraviolet WLED devices', *International Journal of Technology*, vol. 14, no. 3, pp. 501-509, https://doi.org/10.14716/ijtech.v14i3.5904

Tian, W, Hui, X, Li, Y, Dai, J, Fang, Y, Wu, Z & Chen, C 2013, 'Improvement of blue InGaN light-emitting diodes with gradually increased barrier heights from n- to p-layers', *Frontiers of Optoelectronics*, vol. 6, no. 4, pp. 429-434, https://doi.org/10.1007/s12200-013-0342-x

Tran, AMD, Anh, NDQ & Loan, NTP 2020a, 'Enhancing light sources color homogeneity in high-power phosphor-based white LED using ZnO particles', *Telkomnika*, vol. 18, no. 5, pp. 2628-2634, https://doi.org/10.12928/TELKOMNIKA.v18i5.14198

Tran, TC, Anh, NDQ & Loan, NTP 2020b, 'The excellent color quality of phosphor-converted white light-emitting diodes with remote phosphor geometry', *Telkomnika*, vol. 18, no. 5, pp. 2757-2763, https://doi.org/10.12928/telkomnika.v18i5.13575

Tung, HT, Thi, MHN & Anh, NDQ 2024, 'Improved color uniformity in white light-emitting diodes using LILU$(MOO_4)_2$:SM^3+ combined SiO_2 composite', *International Journal of Technology*, vol. 15, no. 1, pp. 8-17, https://doi.org/10.14716/ijtech.v15i1.6165

Verzellesi, G, Saguatti, D, Meneghini, M, Bertazzi, F, Goano, M, Meneghesso, G & Zanoni, E 2013, 'Efficiency droop in InGaN/GaN blue light-emitting diodes: Physical mechanisms and remedies', *Journal of Applied Physics*, vol. 114, no. 7, article 071101, https://doi.org/10.1063/1.4816434

Widiyati, C & Poernomo, H 2018, 'Design of a prototype photoreactor UV-LEDs for radiation vulcanization of natural rubber latex', *International Journal of Technology*, vol. 9, no. 1, pp. 130-141, https://doi.org/10.14716/ijtech.v9i1.1164

Wu, H, Cheng, H, Feng, Y, Chen, X & Wang, Y 2020, 'Luminance mapping of light sources using ray sampling and compression', *Journal of Modern Optics*, vol. 67, no. 2, pp. 99-110, https://doi.org/10.1080/09500340.2019.1697832